

Shape of ammonium chloride dendrite tips at small supersaturation

Andrew Dougherty* and Mayank Lahiri
Dept. of Physics, Lafayette College, Easton PA 18042
(Dated: December 20, 2018)

We report detailed shape measurements of the tips of three-dimensional NH₄Cl dendrites grown from supersaturated aqueous solution. For growth at small supersaturation, we compare three different models: parabolic, parabolic with a fourth-order correction, and power law. None is ideal, but the fourth-order fit appears to provide the most robust description of both the tip shape and position for this material.

PACS numbers: 68.70.+w, 81.10.Dn, 64.70.Dv

I. INTRODUCTION

Dendrites are the most commonly observed microstructural form resulting from the diffusion-limited solidification of non-faceting materials, and they continue to be interesting for both practical and aesthetic reasons. Practically, an improved understanding of dendritic microstructures may enhance the ability to predict and control material properties. Aesthetically, they are an intriguing example of pattern formation under non-linear and non-equilibrium conditions.[1, 2, 3, 4]

Two of the most basic experimental characterizations of a growing dendrite are the tip size and growth speed. Although there is already considerable data available, recent advances in both theory and experimental technique have made more precise comparisons between them possible. Such comparisons have already been made for some pure materials[5, 6], but it is important that they also be made for as broad a range of systems as is reasonable, in order to clarify the roles of various effects such as solution *vs.* thermal growth, and different values of crystalline anisotropy.

In the absence of surface tension, one solution to the diffusive growth problem is a parabolic dendrite with radius of curvature ρ propagating at constant speed v . However, the presence of surface tension, and the instabilities that lead to sidebranching, complicate the problem considerably. Indeed even the most basic issues about the precise tip shape and whether a dendrite actually grows with a constant velocity are still areas of active research[5, 6, 7, 8, 9, 10, 11, 12, 13, 14].

Addressing both of those issues requires unambiguous ways to identify both the tip size and position. In this paper, we consider three different models for the dendrite tip shape and evaluate their use to characterize the growth of NH₄Cl dendrites at small supersaturations.

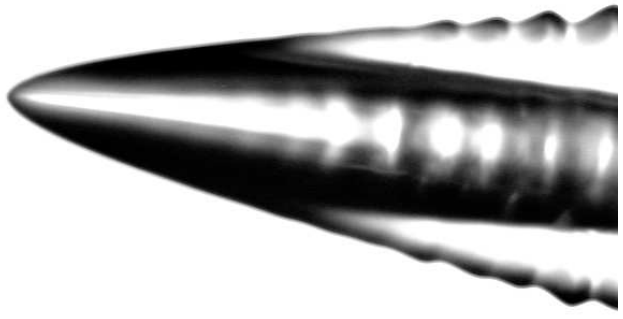


FIG. 1: Dendrite of NH₄Cl. The picture is approximately 400 μm across.

II. BACKGROUND

A typical dendrite of NH₄Cl grown in this study is shown in Fig. 1. Since NH₄Cl has cubic symmetry, four sets of sidebranches grow approximately perpendicular to the main dendrite stem. In Fig. 1, two sets of sidebranches are visible in the plane of the image; two additional branches are growing perpendicular to the plane of the image.

The coordinate system used in this work is defined as follows. The main dendrite stem is used to define the z axis. The growth direction is taken as the negative- z direction, so the solid crystal lies along the positive z axis. The x axis is defined as the direction in the plane of the image perpendicular to z . Lastly, ϕ is defined to be the rotation angle of the crystal around the z -axis. A dendrite with $\phi \approx 45^\circ$ is shown in Fig. 2.

A. Parabolic fit

For diffusion-controlled growth in the absence of surface tension, the Ivantsov solution is a paraboloid of revolution of radius ρ growing at speed v . Once anisotropic surface tension is included, microscopic solvability[3, 15] predicts both the tip size ρ and speed v depend on the crystalline anisotropy ϵ_4 . For a fourfold-symmetric crys-

*doughera@lafayette.edu; <http://www.lafayette.edu/~doughera/>

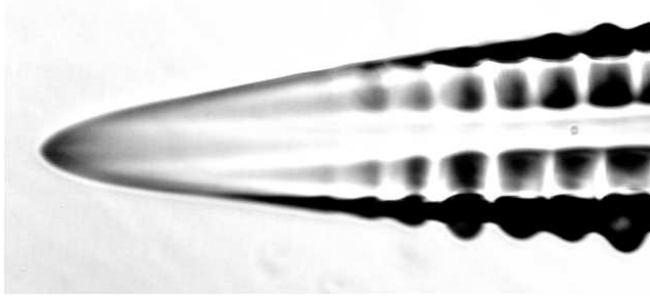


FIG. 2: Dendrite of NH_4Cl with $\phi \approx 45^\circ$. The scale is the same as in Fig 1.

tal such as NH_4Cl , that anisotropy can be expressed in spherical coordinates as[12]

$$\gamma(\Theta, \Phi)/\gamma_0 = 1 + \epsilon_4[4 \cos^4 \Theta + (3 + \cos 4\Phi) \sin^4 \Theta] \quad (1)$$

where γ is the surface free energy, and Θ and Φ are the usual spherical angles.

Although the presence of anisotropic surface tension is critical for the development of the dendritic structure, the overall magnitude of the surface tension is small, so the deviations of the tip shape from parabolic might be expected to be rather small as well. Many experiments, including the landmark experiments of Huang and Glicksman[16], confirm that a parabola is indeed a reasonably good approximation to the tip shape. Experiments on NH_4Br also showed that a parabola is a reasonably good approximation, at least relatively close to the tip[17].

In order to fit the data to a parabola, the data representing the interface positions are first rotated by an angle θ in the plane of the image, and then fit to a parabola of the form

$$z = z_{tip} + \frac{(x - x_{tip})^2}{2\rho}, \quad (2)$$

where (x_{tip}, z_{tip}) is the location of the tip, and ρ is the radius of curvature at the tip.

B. Parabolic fit with fourth-order correction

In the limit of small fourfold-anisotropy, Ben Amar and Brener[18] found that the lowest order correction to the parabolic shape is a fourth-order term proportional to $\cos 4\phi$, where ϕ is the rotation angle around the z axis. Thus, at least close to the tip, the tip shape could be reasonably well described by

$$z = z_{tip} + \frac{(x - x_{tip})^2}{2\rho} - A_4 \cos 4\phi \frac{(x - x_{tip})^4}{\rho^3}, \quad (3)$$

where $A_4 = 1/96$, independent of anisotropy strength[19]. The radius of curvature at the tip is still

given by ρ . Using a somewhat different approach, McFadden, Coriell, and Sekerka[12] found that, to second order in ϵ_4 , $A_4 = \epsilon_4 + 12\epsilon_4^2$, at least very close to the tip. Using an estimate of $\epsilon_4 \approx 0.016$ (the value reported for NH_4Br [17]) this corresponds to $A_4 \approx 0.019$.

C. Power-law

Further back from the tip, the crystalline anisotropy tends to concentrate material into four “fins” such that the shape is no longer well-described by Eq. 3. The width of the fins is predicted[20] to scale as $(z - z_{tip})^{3/5}$.

In this model, we describe the tip shape by

$$z = z_{tip} + \frac{|x - x_{tip}|^{5/3}}{(2\rho)^{2/3}}, \quad (4)$$

where we have included the factor of 2 by analogy with Eq. 2. The parameter ρ still sets a length scale for the dendritic structure, but the curvature at the tip is no longer defined.

Scaling consistent with this prediction was observed in the growth of pure xenon dendrites[14, 21], and in the average shapes of NH_4Cl and pivalic acid dendrites grown from solution[22, 23],

D. Previous Investigations

This work builds on several previous investigations. LaCombe and coworkers studied succinonitrile dendrite tips under a variety of three-dimensional crystal orientations. They evaluated both second order and fourth-order polynomial fits, and concluded that the fourth-order fit worked significantly better.[5, 8] Bisang and Bilgram studied xenon dendrite tips and concluded that a power law of the form Eq. 4 was the most robust fit for that material.[14, 21]

A similar exploration of different tip shape models for dendrites resulting from phase-field simulations was reported by Karma, Lee, and Plapp[11].

E. Experimental Considerations

In order to avoid contamination from sidebranches, only data relatively close to the tip should be used. That is, only data with $(z - z_{tip}) < z_{max}$ is used in the fit. Since sidebranching activity is detectable even for $(z - z_{tip})$ just a few times ρ , (at least for NH_4Br dendrites[24]), z_{max} should not be made too large. On the other hand, z_{max} should not be made too small since the the area around the tip contains the sharpest curvatures and the largest concentration gradients, and hence is the the most subject to optical distortions[5, 17]. Considering both issues, Dougherty and Gollub[17] suggested $z_{max} = 3\rho$ as

a compromise. With more detailed theoretical predictions, and with higher quality imaging, it is now possible to re-examine that compromise for both parabolic and non-parabolic fits.

III. EXPERIMENTS

The experiments were performed with aqueous solutions of ammonium chloride with approximately 36% NH₄Cl by weight. The saturation temperature was approximately 65°C. The solution was placed in a 45 × 12.5 × 2 mm glass cell and sealed with a teflon stopper. The cell was mounted in a massive temperature-controlled copper block surrounded by an insulated temperature-controlled aluminum block, and placed on the stage of an Olympus BH-2 microscope. The entire microscope was enclosed in an insulating box.

The temperature of the outer aluminum block was controlled by an Omega CN-9000 controller to approximately $\pm 1^\circ\text{C}$. The temperature of the inner copper block was controlled directly by computer. A thermistor in the block was connected via a Kiethley 2000 digital multimeter to the computer, where the resistance was converted to temperature. The computer then controlled the heater power supply using a software version of a proportional-integral controller. This allowed very flexible control over not just the temperature, but also over any changes in the temperature, such as those used to initiate growth. The temperature of the sample was stable to within approximately $\pm 5 \times 10^{-4}^\circ\text{C}$.

A charged coupled device (CCD) camera was attached to the microscope and images were acquired directly into the computer with a Data Translation DT3155 frame grabber with a resolution of 640 × 480 pixels. The ultimate resolution of the images was $0.63 \pm 0.01 \mu\text{m}/\text{pixel}$. As a backup, images were also recorded onto video tape for later use.

Dendritic crystals were obtained in the following manner. First, the solution was heated to dissolve all the NH₄Cl, stirred to eliminate concentration gradients, and then cooled to initiate growth. Typically, many crystals would nucleate. An automated process was set up to acquire an image and then slowly adjust the temperature until all but the largest crystal had dissolved.

This isolated crystal was allowed to stabilize for several days. The temperature was then reduced by 0.77 °C and the crystal was allowed to grow. The crystal was initially approximately spherical, but due to the cubic symmetry of NH₄Cl, six dendrite tips would begin to grow. The tip with the most favorable orientation was followed, and images were recorded at regular intervals.

The interface position was determined in the same manner as in Ref. [17]. Briefly, the intensity in the image was measured on a line perpendicular to the interface. A typical intensity profile from Fig. 1 is shown in Fig. 3. Over the range of a few pixels, the intensity changes rapidly from bright to dark. Deeper inside the

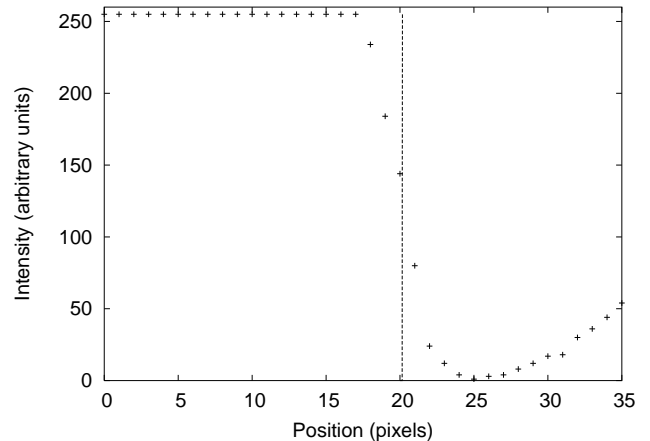


FIG. 3: Image intensity along a line perpendicular to the interface in Fig. 1. The vertical line shows the interpolated interface position.

crystal, the intensity begins to rise again. (This corresponds to the brighter areas inside the crystal in Fig. 1.) In the bright-to-dark transition region, we fit a straight line to the intensity profile. We define the interface as the location where the fitted intensity is the average of the high value outside the crystal and the low value just inside the crystal. This fitting procedure interpolates intensity values and allows a reproducible measure of the interface to better than one pixel resolution. It is also insensitive to absolute light intensity levels, to variations in intensity across a single image, and to variations in intensity *inside* the crystal well away from the interface.

This method works best if the image is scanned along a line perpendicular to the interface. Since the position and orientation of the interface are originally unknown, an iterative procedure is used until subsequent iterations make no significant change to the fit.

Specifically, we start with an initial estimate of the size, location, and orientation of the tip, and use that to scan the image to obtain a list of interface positions up to a distance z_{max} back from the tip (where z_{max} is some multiple of ρ). We next rotate the data by an angle θ in the $x - z$ plane and perform a non-linear regression on Eq. 2, 3, or 4 to determine the best fit values for x_{tip} , z_{tip} , ρ , and A_4 (if applicable), and the corresponding χ^2 value. We then repeat with different θ values and minimize χ^2 using Brent's algorithm[25]. This completes one iteration of the fitting procedure. We use this result to rescan the image along lines perpendicular to the interface to obtain a better estimate of the interface location and begin the next iteration. The procedure usually converges fairly rapidly. Even for a relatively poor initial estimate, it typically takes fewer than 20 iterations.

There are some subtleties to the procedure worth noting. First, for a typical crystal in this work such as in Fig. 1, only about 120 data points are involved in the fit for $z_{max} = 6\rho$. For the fourth-order fit with five free

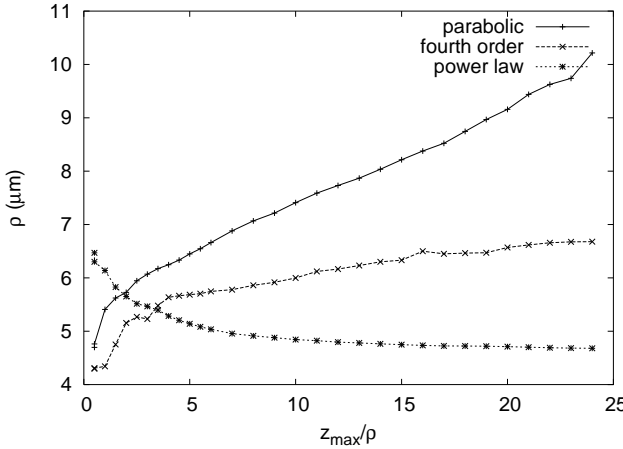


FIG. 4: Best fit value of ρ as a function of z_{max}/ρ for the crystal shown in Fig. 1. The curves are for a parabolic fit (+), a fourth-order fit (x), and a power-law fit (*).

parameters, there are often a number of closely-spaced local minima in the χ^2 surface, with tip positions and radii varying by a few hundredths of a micrometer. If the iterative procedure enters a limit cycle instead of settling down to a single final value, we select the element from that limit cycle with the minimum χ^2 . Second, it is worth noting that a generic fourth-order polynomial fit is inappropriate for Eq. 3, since (after rotation) there are only four parameters to fit: x_{tip} , y_{tip} , ρ , and A_4 . Primarily to ensure programming consistency and correctness, we use the same nonlinear regression technique on all three models, even though (after rotation) Eq. 2 can be fit by linear regression. Finally, we have no way to control or precisely measure the orientation angle ϕ of the crystals in our system.

IV. RESULTS

The best estimates of ρ as a function of z_{max}/ρ for the crystal in Fig. 1 are shown in Fig. 4. The corresponding χ^2 values are shown in Fig. 5.

None of the fits is robust very close to the tip, indicating that the actual tip shape is not well-described by any of the candidate functions. The parabolic fit also gets rapidly worse for z_{max} greater than about 5ρ . The fourth-order fit appears to have a plateau between roughly 5 and 8ρ , but ρ gradually increases with z_{max} , and the χ^2 value rapidly increases for $z_{max} > 10\rho$. By contrast, the power law fit gives relatively stable values at large z_{max} for both ρ and χ^2 .

A second important consideration is the degree to which each fit accurately describes the tip *location*. This is illustrated in Fig. 6, which shows x_{tip} for each fit. Here, the fourth-order fit is clearly the most reliable.

Finally, Fig. 7 shows the original data along with each of the three model fits superposed for $z_{max} = 6\rho$. Of the

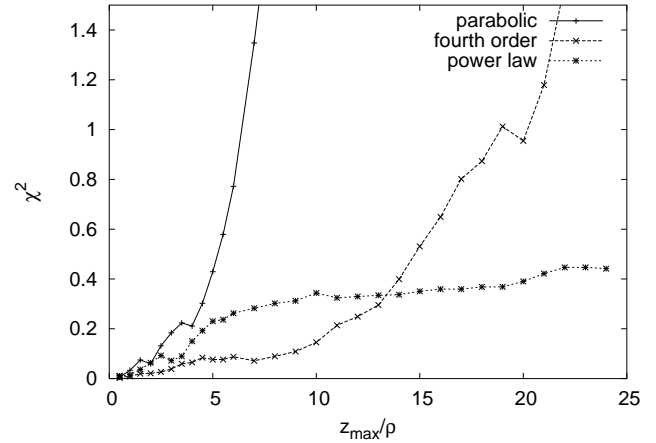


FIG. 5: Values of χ^2 for the best fit as a function of z_{max}/ρ for the crystal shown in Fig. 1. The curves are for a parabolic fit (+), a fourth-order fit (x), and a power-law fit (*).

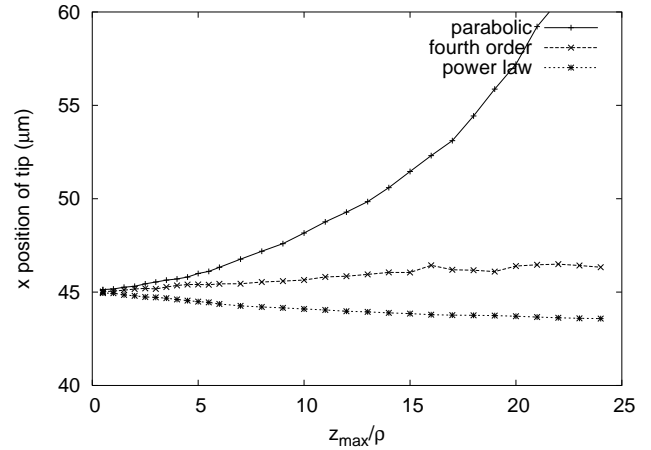


FIG. 6: Best-fit values for the x -position of the tip as a function of z_{max}/ρ for the crystal shown in Fig. 1. Symbols are as in the previous figures.

three fits, the fourth-order does the best job of capturing both the tip location and shape.

For the value of $z_{max} = 6\rho$, we find $A_4 = 0.004 \pm 0.001$, which is similar to that measured by LaCombe *et al.* for succinonitrile[5, 8], and to that obtained in the simulations by Karma, Lee, and Plapp[11]. This value for A_4 is less than the value of $1/96$ predicted by Brener[19], and also significantly less than the value of 0.019 estimated by McFadden, Coriell, and Sekerka[12]. (It is worth noting, however, that this latter prediction is only intended to be valid close to the tip, where our fit is not robust.)

The results are fairly similar for the crystal shown in Fig. 2, which has $\phi \approx 45^\circ$. The best estimates of ρ as a function of z_{max}/ρ for the three fits are shown in Fig. 8, and the corresponding χ^2 values are shown in Fig. 9.

Both the parabolic and fourth order models fit reasonably well for z_{max} between roughly 5 and 8ρ . Indeed

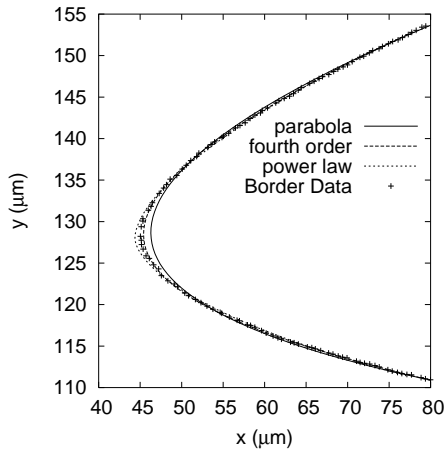


FIG. 7: Best-fit parabolic (solid), fourth-order (dashed), and power-law (dotted) curves for $z_{max} = 6\rho$, along with the original border (+) for the crystal shown in Fig. 1. Near the tip, the parabolic fit is too far to the right, while the power law fit is too far to the left. The fourth-order fit matches the tip region fairly well.

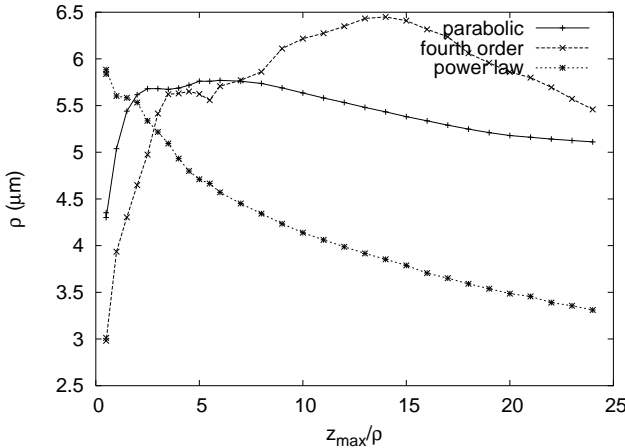


FIG. 8: Best fit value of ρ as a function of z_{max}/ρ for the crystal shown in Fig. 2. The curves are for a parabolic fit (+), a fourth-order fit (x), and a power-law fit (*).

within that range, for the entire run from which Fig. 2 was taken, the value for A_4 is 0.0007 ± 0.0009 , consistent with zero. In contrast, the power law is a poor fit.

One significant problem with this measurement is that the image in Fig. 2 is a projection of the true three-dimensional shape. This is discussed in Ref. [5, 8] and in considerably more detail in Ref. [11], but, in general, our findings are consistent with those of LaCombe *et al.*[5, 8].

V. CONCLUSIONS

We have considered three different models: parabolic, parabolic with a fourth-order correction, and power law.

None is ideal, but for the system considered here, a fourth-order fit with $z_{max} = 6\rho$ gives a reasonably robust fit. For the crystal in Fig. 1, the coefficient of the fourth-order term is $A_4 = 0.004 \pm 0.001$, significantly less than the theoretically expected value. The fourth-order fit also handles rotated crystals, such as those in Fig. 2, fairly robustly. These findings are consistent with those of LaCombe *et al.*[5, 8] for succinonitrile dendrites.

By contrast, the power-law fit was reasonably robust for $\phi \approx 0$, in agreement with the results of Bisang and Bilgram[14, 21] for xenon dendrites, but it did not work as well for crystals with $\phi \approx 45^\circ$. One other problem with the power law fit is that it does not accurately describe the crystal shape near the tip. Accordingly, it may be more difficult to use a power law fit to look for both the onset of sidebranching and possible tip oscillations.

Two remaining issues may be relevant for all of the models. First, the extent to which optical distortions near the tip affect the results has not been addressed. Specifically, since both the concentration gradients and the interfacial curvature are largest near the tip, the data closest to the tip are the least reliable[5, 17]. Second, the extent to which all of these fits are contaminated by early sidebranches needs to be investigated. This may be especially important in characterizing the emergence of sidebranches as well as in studies of possible tip oscillations.

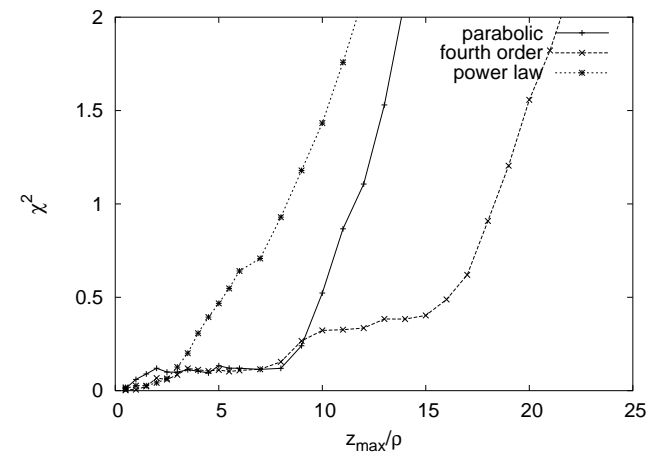


FIG. 9: Values of χ^2 for the best fit as a function of z_{max}/ρ for the crystal shown in Fig. 2. The curves are for a parabolic fit (+), a fourth-order fit (x), and a power-law fit (*).

[1] W. Boettinger, S. Coriell, A. Greer, A. Karma, W. Kurz, M. Rappaz, and R. Trivedi, *Acta Mater.* **48**, 43 (2000).

[2] M. E. Glicksman and S. P. March, in *Handbook of Crystal Growth*, edited by D. J. T. Hurle (Elsevier Science, 1993), p. 1081.

[3] D. A. Kessler, J. Koplik, and H. Levine, *Adv. Phys.* **37**, 255 (1988).

[4] J. Langer, *Rev. Mod. Phys.* **52**, 1 (1980).

[5] J. C. LaCombe, M. B. Koss, V. E. Fradkov, and M. E. Glicksman, *Phys. Rev. E* **52**, 2778 (1995).

[6] U. Bisang and J. Bilgram, *J. Cryst. Growth* **166**, 212 (1996).

[7] U. Bisang and J. Bilgram, *J. Cryst. Growth* **166**, 207 (1996).

[8] M. Koss, J. Lacombe, L. Tennenhouse, M. Glicksman, and E. Winsa, *Metall. and Mater. Trans. A* **30**, 3177 (1999).

[9] J. Lacombe, M. Koss, D. Corrigan, A. Lupulescu, L. Tennenhouse, and M. Glicksman, *J. Cryst. Growth* **206**, 331 (1999).

[10] J. Lacombe, M. Koss, and M. Glicksman, *Phys. Rev. Lett.* **83**, 2997 (1999).

[11] A. Karma, Y. Lee, and M. Plapp, *Phys. Rev. E* **61**, 3996 (2000).

[12] G. B. McFadden, S. R. Coriell, and R. F. Sekerka, *Acta Mater.* **48**, 3177 (2000).

[13] J. C. LaCombe, M. Koss, J. E. Frei, C. Giumentarri, A. O. Lupulescu, and M. E. Glicksman, *Phys. Rev. E* **65**, 031604 (2002).

[14] U. Bisang and J. Bilgram, *Phys. Rev. E* **54**, 5309 (1996).

[15] D. A. Kessler and H. Levine, *Acta Metall.* **36**, 2693 (1988).

[16] M. E. Glicksman and S.-C. Huang, *Acta Metall.* **29**, 701 (1981).

[17] A. Dougherty and J. P. Gollub, *Phys. Rev. A* **38**, 3043 (1988).

[18] M. B. Amar and E. Brener, *Phys. Rev. Lett.* **71**, 589 (1993).

[19] E. Brener and V. I. Mel'nikov, *JETP* **80**, 341 (1995).

[20] E. Brener, *Phys. Rev. Lett.* **71**, 3653 (1993).

[21] U. Bisang and J. H. Bilgram, *Phys. Rev. Lett.* **75**, 3898 (1995).

[22] A. Dougherty and R. Chen, *Phys. Rev. A* **46**, R4508 (1992).

[23] A. Dougherty and A. Gunawardana, *Phys. Rev. E* **50**, 1349 (1994).

[24] A. Dougherty, P. D. Kaplan, and J. P. Gollub, *Phys. Rev. Lett.* **58**, 1652 (1987).

[25] W. H. Press, S. A. Teukolsky, W. T. Vetterling, and B. P. Flannery, *Numerical Recipes in C* (Cambridge University Press, 1992).